

MARSHALL
GRANT

1N-25-CR

148510

49P

SEMI-ANNUAL REPORT
DEVELOPMENT OF A COMPUTERIZED ANALYSIS
FOR
SOLID PROPELLANT COMBUSTION INSTABILITY WITH TURBULENCE
NAG8-627

by

T. J. Chung and O. Y. Park

Department of Mechanical Engineering
The University of Alabama in Huntsville

prepared for

NASA/MSFC

(NASA-CR-182351) DEVELOPMENT OF A
COMPUTERIZED ANALYSIS FOR SOLID PROPELLANT
COMBUSTION INSTABILITY WITH TURBULENCE
Semiannual Report (Alabama Univ.) 49 p

N88-25497

Unclas
CSCL 21B G3/25 0148510

May, 1988

ABSTRACT

A multi-dimensional numerical model has been developed for the unsteady state oscillatory combustion of solid propellants subject to acoustic pressure disturbances. Including the gas phase unsteady effects, the assumption of uniform pressure across the flame zone, which has been conventionally used, is relaxed such that a higher frequency response in the long flame of a double-base propellant can be calculated. The formulation is based on a premixed, laminar flame with a one-step overall chemical reaction and the Arrhenius law of decomposition with no condensed phase reaction. In a given geometry, the Galerkin finite element solution shows the strong resonance and damping effect at the lower frequencies, similar to the result of Denison and Baum. Extended studies deal with the higher frequency region where the pressure varies in the flame thickness. The nonlinear system behavior is investigated by carrying out the second order expansion in wave amplitude when the acoustic pressure oscillations are finite in amplitude. Offset in the burning rate shows a negative sign in the whole frequency region considered, and it verifies the experimental results of Price. Finally, the velocity coupling in the two-dimensional model is discussed.

NOMENCLATURE

a	speed of sound
B	frequency factor for gas phase reaction
C_p	specific heat at constant pressure for gas
C_s	specific heat of solid
E	gas phase activation energy
E_s	surface activation energy
F	eigenvector
G	source term in numerical formulation
h	heat of combustion per unit mass
H	heat of reaction
I	order of perturbation
k	thermal conductivity
ℓ	characteristic flame length
L	latent heat of vaporization
m	mass flux
M_b	Mach number
n	order of chemical reaction
P	pressure
Pr	Prandtl number
r	burning rate
R	gas constant
R_c	dimensionless distance from surface in Eq. (22)
t	time
T	temperature
u	axial gas velocity
u_i	velocity vector

u_c	core velocity in Eq. (22)
v	normal gas velocity
w	reaction rate
x	axial distance parallel to the surface
X	solution vector
y	normal distance from the surface
Y	mass fraction of fuel species
z	oxidizer-fuel ratio
α	thermal diffusivity
β	ratio of solid to gas density
δ	temperature exponent in Eq. (7)
γ	specific heat ratio
ϵ	perturbation parameter
ζ	$= k_s^* C_p^* / k^* C_s^*$
λ	eigenvalue
λ_γ	Lagrange multiplier
ξ	$= k^* / k_s^*$
ρ	density
ω	frequency

Subscripts and Superscripts

*	dimensional quantity
-	steady-state mean value
\wedge	spatial variable
(i)	i^{th} order perturbation coefficient
+	gas side of interface
-	solid side of interface
c	propellant cold side

D time-dependent variable
i,j vector quantity
I time-independent variable
O mean value at flame edge
s solid phase
 α, β finite element global node number
† complex conjugate

1. INTRODUCTION

An accurate analysis of combustion instability resulting from the oscillatory burning of solid propellants has long been of major concern. Such an analysis is characterized by the acoustic admittance or response function, a proper measure of instability. However, experimental measurements of the coefficients are difficult; thus, it is desirable that analytical or numerical calculations be implemented whenever possible.

Most of the past investigations on combustion instability have been centered around a one-dimensional quasi-steady analysis limited to pressure coupling [1-19]. The representative studies were accomplished by Hart and McClure [2], Denison and Baum [4], and Culick [12-14]. Culick's review article [12] on homogeneous propellants summarizes the state-of-the-art up to the late 1960's and discusses the limitations of the analyses. Recently, several works concerning unsteady state problems have been attempted [20-27]. T'ien [21] introduces improved gas dynamics in order to recover the quasi-steady limitations by considering both gas and solid phases in an unsteady manner. However, the pressure is

still assumed to be constant and a function of time only, which has generally been used. Consequently, as indicated, in the case of the long flame of a double-base propellant, application of the model is limited to lower frequencies.

Flandro [23,24] presents the first attempt to examine the response functions under the effect of incident acoustic waves in a two-dimensional analysis. A detailed formulation is extended to the second order perturbation system in terms of the Prandtl number and the Mach number. The effects of viscosity and heat transfer in the gas phase are included. The numerical results for the first order system appear to be comparable to those of T'ien [21]; however, the results of the second order response function are not clear. Moreover, details of matching conditions are not given. The requirements for a more realistic model of combustion instability have lead to quite a number of rigorous studies. One recent work deals with the heterogeneous propellants summarized in Cohen's review paper [30-33].

The major discussions of the acoustic admittance or response function in the literature are concerned with pressure coupling usually applicable in the linear stability. Computations of the response function for velocity coupling are important in a nonlinear process; however, they remain in a state of infancy, although some initial attempts toward this subject have been made [34-38]. Observations indicate that combustion oscillations are time-dependent and often nonlinear, as influenced by turbulent flow fields which may lead to erosive burning and unstable oscillations. Since the complicated physical phenomena cannot be

described analytically, some approximations and simplifications are still introduced to the theoretical formulations in the numerical analyses. Recently, Chung and Kim [26] introduced the effect of radiative heat transfer on the combustion instability in solid rocket motors based on the research of Chung and Kim [27]. Further research has been reported concerning the calculation of response functions in multi-dimensional combustion phenomena [28]. The finite element method is introduced and complicated boundary conditions are handled easily by means of Lagrange multipliers [29].

On the other hand, much experimental effort has been devoted to understanding the oscillatory combustion mechanism using the T-burner and L*-burner [39-42]. Extensive experiments may be found in the recent series of papers conducted by Levine and Baum [43,44]. Also, in the work of Caveny et al. [45], the oscillatory velocities in the solid propellant flames subject to pressure coupling are measured directly using the laser Doppler velocimetry instrumentation.

The purpose of the present study is to examine the combustion instability induced by acoustic disturbances in the multi-dimensionally unsteady state in such a way that the upper limit of the acoustic wave frequency, above which an analysis with the assumption of the uniform pressure field in the flame zone cannot be applicable, is relaxed. Thus, very high pressure burnings (where any dynamic effects are to be important) and the long gas flame (such as burning of double-base solid propellants) could be possibly sought.

For small amplitude oscillations, the nonsteady governing equations are linearized by means of the first and second order perturbation expansions and solved numerically using the finite element method. The theoretical model is still based on a homogeneous propellant, Lewis number of unity, a second-order, single-step forward chemical reaction, and vaporization in an Arrhenius fashion, with no erosive burning.

2. ANALYSIS

For the simplicity of the combustion modeling of solid propellants, the gaseous flame is assumed to be multi-dimensional, premixed laminar, and calorically perfect, and a one-step forward chemical reaction occurs. The combustion of a solid propellant is approximated by the Arrhenius law. The Lewis number is given as unity for the explicit relation between concentration and temperature. Thus, the conservation laws for the multi-component reactive system in the gas phase are represented as follows:

Continuity

$$\frac{\partial \rho}{\partial t} + (\rho u_i)_{,i} = 0 \quad (1)$$

Momentum

$$\rho \frac{\partial u_i}{\partial t} + \rho u_{i,j} u_j + \frac{1}{\gamma M_b^2} P_{,i} - \text{Pr} \left(u_{i,jj} + \frac{1}{3} u_{j,ii} \right) = 0 \quad (2)$$

Energy

$$\rho \frac{\partial T}{\partial t} + \rho u_i T_{,i} - \frac{\gamma - 1}{\gamma} \frac{\partial P}{\partial t} - T_{,ii} - wh = 0 \quad (3)$$

Species

$$\rho \frac{\partial Y}{\partial t} + \rho u_i Y_{,i} - Y_{,ii} + w = 0 \quad (4)$$

State

$$P = \rho T \quad (5)$$

where the commas denote partial derivatives, the repeated indices imply summing, Pr is the Prandtl number, and Y represents the fuel mass fraction. Note that only one out of three species equations (fuel, oxidizer, and product) is taken into account from the simple chemical reaction model [21]. The following characteristic parameters are used to render the above equations dimensionless:

$$\begin{aligned} \rho &= \rho^*/\rho_0^* \quad , \quad P = P^*/P_0^* \quad , \quad T = T^*/T_0^* \\ u_i &= u_i^*/v_0^* \quad , \quad t = t^*v_0^*/\ell^* \quad , \quad x_i = x_i^*/\ell^* \\ M_b &= v_0^*/a_0^* \quad , \quad h = h^*/C_p^*T_0^* \quad , \quad w = w^*a^*/v_0^{*2} \end{aligned} \quad (6)$$

in which ℓ^* is the flame thickness given by α^*/v_0^* , with α^* being the thermal diffusivity, M_b represents the Mach number; k^* , the thermal conductivity; a_0^* , the speed of sound; h^* , the combustion heat release; and w^* , the reaction rate, whose dimensionless form

is

$$w = BzT^{\delta} \left(\frac{P}{T} \right)^n Y^n \exp[-E/T] \quad (7)$$

with z denoting the oxidizer-fuel ratio; n , the order of chemical reaction; E , the activation energy given by $E = E^*/RT_0^*$; and B , the rate constant. The superscript $*$ represents dimensional quantities and subscript zero gives the mean value at the flame edge.

The solid propellant is assumed to be homogeneous, with no condensed phase chemical reaction. The dimensionless form of the heat transfer equation in the solid phase is

$$\beta \frac{\partial T_s}{\partial t} + u_1 T_{s,1} - \zeta T_{s,11} = 0 \quad (8a)$$

Furthermore, assuming that the heat transfer is one-dimensional gives,

$$\beta \frac{\partial T_s}{\partial t} + r \frac{\partial T_s}{\partial y} - \zeta \frac{\partial^2 T_s}{\partial y^2} = 0 \quad (8b)$$

where

$$\begin{aligned} \beta &= \rho_s^*/\rho_0^* \quad , \quad \zeta = k_s^* C_p^*/k^* C_s^* \\ r &= r^*/\bar{r}^* \quad \text{with} \quad \bar{r}^* = \rho_0^* v_0^*/\rho_s^* \end{aligned}$$

Here, r denotes the burning rate at the solid surface and subscript s represents the solid phase. The decomposition process of the solid propellant at the surface is assumed to

follow an Arrhenius law; thus,

$$r = \exp \left[-E_s \left(\frac{1}{T_s} - \frac{1}{\bar{T}_s} \right) \right] \quad (9)$$

in which E_s is the dimensionless surface activation energy, $E_s = E_s^*/RT_0^*$, and \bar{T}_s is the mean temperature at the surface. The solid-gas interface boundary conditions are determined by the dimensionless mass and energy balances across the interface, such that

$$\left(\frac{\partial T}{\partial y} \right)_+ = \frac{1}{\xi} \left(\frac{\partial T}{\partial y} \right)_- + rL \quad (10)$$

with $\xi = k^*/k_s^*$ and $L = (H_+^* - H_-^*)/C_p^*T_0^*$. Here, L is the latent heat of vaporization of the propellant and H^* denotes the enthalpy changes. The subscripts $+$ and $-$ represent the gas and solid side at the interface, respectively.

When a small pressure disturbance occurs in the combustion chamber, every field variable will be disturbed from its steady-state value and can be expressed in the form,

$$F = F^{(0)} + \epsilon F^{(1)} + \epsilon^2 F^{(2)} + \dots \quad (11)$$

where $F = \{\rho, u_i, T, Y, P\}$ and ϵ represents the perturbation parameter. The superscripts in the parentheses indicate the perturbation order. Furthermore, assuming sinusoidal fluctuation of pressure with time renders the variables in a different form:

$$F^{(I)} = \hat{F}^{(I)} e^{iI\omega t}, \quad I = 1, 2, \dots \quad (12)$$

It is important to recognize that the sources in the second order consist of inhomogeneous terms that describe the nonlinearities in terms of the product of two first order variables. Considering the physical quantity of $F^{(1)}$ leads to the separation of each inhomogeneous term into a time-independent term and a term oscillating at the frequency of the second harmonic, i.e.,

$$F_1^{(1)} F_2^{(1)} = \frac{1}{2} (\hat{F}_1^{(1)\dagger} \hat{F}_2^{(1)} + \hat{F}_1^{(1)} \hat{F}_2^{(1)} e^{i2\omega t}) \quad (13)$$

with the dagger representing the complex conjugate.

Consequently, the dependent variable $F^{(2)}$ may be rewritten as

$$F^{(2)} = \hat{F}_I^{(2)} + \hat{F}_D^{(2)} e^{i2\omega t} \quad (14)$$

For a higher order, the same argument is applicable.

Substituting Eqs. (11)-(14) into Eqs. (1)-(5) and rearranging separately in the order of perturbation yield the final form of the governing equations corresponding to each order.

Steady-State Governing Equations

The one-dimensional steady-state governing equations are given as follows:

Continuity

$$\rho^{(0)} v^{(0)} = 1 \quad (15)$$

Energy

$$\frac{\partial T^{(0)}}{\partial y} - \frac{\partial^2 T^{(0)}}{\partial y^2} = w^{(0)} h \quad (16)$$

Species

$$\frac{\partial Y^{(0)}}{\partial y} - \frac{\partial^2 Y^{(0)}}{\partial y^2} = -w^{(0)} \quad (17)$$

State

$$\rho^{(0)} T^{(0)} = 1 \quad (18)$$

Note that the uniform pressure is retained throughout the flame thickness ($P^{(0)} = 1$), and from Eqs. (6) and (11), both the dependent variables, $\rho^{(0)}$ and $T^{(0)}$, are equal to unity at the flame edge, which is far from the origin on the scale of ℓ^* .

From Eqs. (15) and (18), we have

$$v^{(0)} = T^{(0)} \quad (19)$$

and from Eqs. (16) and (17), $Y^{(0)}$ can be expressed as

$$Y^{(0)} = \frac{1}{h} (1 - T^{(0)}) \quad (20)$$

Therefore,

$$w^{(0)} = \frac{1}{h^2} Bz \left(\frac{1 - T^{(0)}}{T^{(0)}} \right)^2 \exp[-E/T^{(0)}] \quad (21)$$

where $\delta = 0$ and the second order chemical reaction is assumed.

Now, the equations are expressed in terms of temperature in the steady-state; thus, only the solution of Eq. (16) is required. Flandro [23] suggests a simple analytical model of the

mean flow field to facilitate multi-dimensional analysis in the higher order system. This model is given in the form

$$u_i^{(0)} = u_c [1 - \exp(-y/R_c)] \hat{i} + v^{(0)} \hat{j} \quad (22)$$

Here, u_c describes the flow speed along the local streamline and R_c is a dimensionless distance from the solid surface. The following boundary conditions are used in the steady-state solution:

At the flame edge,

$$y^{(0)} = 0 \quad (23)$$

$$T^{(0)} = 1 \quad (24a)$$

or

$$\frac{dT^{(0)}}{dy} = 0 \quad (24b)$$

At the solid phase, Eq. (8) gives

$$T_s^{(0)} = (\bar{T}_s - T_c) e^{y/\xi} + T_c \quad (25)$$

where T_c is the propellant cold side temperature. The continuous temperature condition at the interface requires that

$$T_{s-}^{(0)} = T_{s+}^{(0)} = \bar{T}_s \quad (26)$$

The matching condition across the interface can be obtained by substituting Eq. (25) into Eq. (10), which yields

$$\left. \frac{dT^{(0)}}{dy} \right|_+ = \frac{\bar{T}_s - T_c}{\xi} + L \quad (27)$$

In solving Eq. (16), note that a correct rate constant B in Eq. (21) has to be determined such that the system satisfies the boundary conditions at the flame edge as well as at the interface.

Higher Order Governing Equations

The higher order governing equations can be expressed in a single form because only the source terms are different from each other. Presenting the source terms on the right-hand side of the equations in terms of G_s , the governing equations are represented as follows:

Continuity

$$iI\omega \hat{\rho}^{(1)} + (\rho^{(0)} \hat{u}_1^{(1)} + \hat{\rho}^{(1)} u_1^{(0)})_{,1} = G_1 \quad (28)$$

Momentum

$$iI\omega \rho^{(0)} \hat{u}_1^{(1)} + [\rho^{(0)} u_{1,j}^{(0)} \hat{u}_j^{(1)} + \rho^{(0)} \hat{u}_{1,j}^{(1)} u_j^{(0)} + \hat{\rho}^{(1)} u_{1,j}^{(0)} u_j^{(0)}] \\ + \frac{1}{\gamma M_b^2} \hat{p}_{,1}^{(1)} - Pr \left[\hat{u}_{1,jj}^{(1)} + \frac{1}{3} \hat{u}_{j,11}^{(1)} \right] = G_{21} \quad (29)$$

Energy

$$iI\omega \rho^{(0)} \hat{T}^{(1)} + [\rho^{(0)} u_1^{(0)} \hat{T}_{,1}^{(1)} + \rho^{(0)} \hat{u}_1^{(1)} T_{,1}^{(0)} + \hat{\rho}^{(1)} u_1^{(0)} T_{,1}^{(0)}] \\ - iI\omega \frac{\gamma - 1}{\gamma} \hat{p}^{(1)} - \hat{T}_{,11}^{(1)} - \hat{w}^{(1)} h = G_3 \quad (30)$$

Species

$$iI\omega \rho^{(0)} \hat{Y}^{(1)} + [\rho^{(0)} u_1^{(0)} \hat{Y}_{,1}^{(1)} + \rho^{(0)} \hat{u}_1^{(1)} Y_{,1}^{(0)} + \hat{\rho}^{(1)} u_1^{(0)} Y_{,1}^{(0)}]$$

$$-\hat{Y}_{,11}^{(1)} + \hat{W}^{(1)} = G_4 \quad (31)$$

State

$$\hat{P}^{(1)} - \rho^{(0)}T^{(1)} - \hat{\rho}^{(1)}T^{(0)} = G_5 \quad (32)$$

and the reaction rate is given by

$$\hat{W}^{(1)} = W^{(0)} \left[\frac{2}{\rho^{(0)}} \hat{\rho}^{(1)} + \frac{E}{T^{(0)2}} \hat{T}^{(1)} + \frac{2}{Y^{(0)}} \hat{Y}^{(1)} \right] + G_6 \quad (33)$$

Here, G_s is given as follows: for the first order system ($I=1$),
 $G = 0$; for the second order system ($I=2$),

$$G_1 = -(\hat{\rho}^{(1)} \hat{u}_i^{(1)})_{,i}$$

$$G_{2i} = -\{i\omega \hat{\rho}^{(1)} \hat{u}_i^{(1)} + \rho^{(0)} \hat{u}_{i,j}^{(1)} \hat{u}_j^{(1)} + \hat{\rho}^{(1)} u_{i,j}^{(0)} \hat{u}_j^{(1)} \\ + \hat{\rho}^{(1)} \hat{u}_{i,j}^{(1)} u_j^{(0)}\}$$

$$G_3 = -\{i\omega \hat{\rho}^{(1)} \hat{T}^{(1)} + \rho^{(0)} \hat{u}_i^{(1)} \hat{T}_{,i}^{(1)} + \hat{\rho}^{(1)} u_i^{(0)} \hat{T}_{,i}^{(1)} \\ + \hat{\rho}^{(1)} \hat{u}_i^{(1)} T_{,i}^{(0)}\}$$

$$G_4 = -\{i\omega \hat{\rho}^{(1)} \hat{Y}^{(1)} + \rho^{(0)} \hat{u}_i^{(1)} \hat{Y}_{,i}^{(1)} + \hat{\rho}^{(1)} u_i^{(0)} \hat{Y}_{,i}^{(1)} \\ + \hat{\rho}^{(1)} \hat{u}_i^{(1)} Y_{,i}^{(0)}\}$$

$$G_5 = \hat{\rho}^{(1)} \hat{T}^{(1)}$$

$$G_6 = W^{(0)} \left\{ \left(\frac{\hat{\rho}^{(1)}}{\rho^{(0)}} \right)^2 + \frac{2E}{\rho^{(0)} T^{(0)2}} \hat{\rho}^{(1)} \hat{T}^{(1)} + \frac{4}{\rho^{(0)} Y^{(0)}} \hat{\rho}^{(1)} \hat{Y}^{(1)} \right. \\ \left. + \frac{E}{T^{(0)}} \left(\frac{E}{2T^{(0)}} - 1 \right) \left(\frac{\hat{T}^{(1)}}{T^{(0)}} \right)^2 + \frac{2E}{Y^{(0)} T^{(0)2}} \hat{Y}^{(1)} \hat{T}^{(1)} + \left(\frac{\hat{Y}^{(1)}}{Y^{(0)}} \right)^2 \right\} \quad (34)$$

Note that, including the pressure coupling, the velocity coupling is significant in the source terms.

At the solid phase, Eq. (8) gives

$$iI\omega\beta\hat{T}_s^{(1)} + r^{(0)} \frac{\partial\hat{T}_s^{(1)}}{\partial y} + \hat{r}^{(1)} \frac{\partial T_s^{(0)}}{\partial y} - \zeta \frac{\partial^2\hat{T}_s^{(1)}}{\partial y^2} = G_7 \quad (35)$$

with

$$G_7 = -\hat{r}^{(1)} \frac{\partial\hat{T}_s^{(1)}}{\partial y}$$

Linearizing Eq. (9) results in

$$\hat{r}^{(1)} = r^{(0)} c_1 (\hat{T}_s^{(1)} + G_8) \quad (36)$$

where

$$G_8 = \left(\frac{c_1}{2} - \frac{1}{\bar{T}_s} \right) \hat{T}_s^{(1)2}$$

Substituting Eq. (36) into Eq. (35) and solving analytically yield

$$\hat{T}_+^{(1)} = \left(\frac{\partial\hat{T}^{(1)}}{\partial y} \Big|_+ + G_9 \right) \left[\frac{\lambda_1}{\xi} \left(1 + \frac{c_1 c_2}{iI\omega\beta} \right) - \frac{c_1 c_2}{iI\omega\beta\xi} + c_1 L \right]^{-1} \quad (37)$$

in which

$$G_9 = \frac{c_3 c_2}{iI\omega\beta\xi} \left(-\lambda_2 + \frac{1}{\xi} \right) + \frac{1}{\xi} \left(\lambda_2 c_4 + c_5 - \frac{c_4}{\xi} \right) - c_3 L$$

and

$$\lambda_1 = \frac{1}{2\zeta} [1 + (1 + i4I\omega\beta\zeta)^{1/2}]$$

$$c_1 = E_s / \bar{T}_s^2$$

$$c_2 = \frac{1}{\zeta} (\bar{T}_s - T_c)$$

$$c_3 = c_1 \left(\frac{c_1}{2} - 1 \right) \hat{T}^{(1)2}$$

$$c_4 = - \frac{c_2 \hat{r}^{(1)2}}{2\omega^2 \beta^2 \zeta}$$

$$c_5 = \frac{\lambda_1(\lambda_2 - \lambda_1)}{(\zeta\lambda_1^2 - \lambda_1 - i2\omega\beta)} \hat{r}_1^{(1)} \left(\hat{T}_s^{(1)} + \frac{c_2 \hat{r}^{(1)}}{i\omega\beta} \right)$$

Equation (37) gives a boundary condition at the surface; other conditions are as follows:

At the flame edge,

$$\hat{y}^{(1)} = 0 \quad (38)$$

Assumption of an isentropic flow near the flame edge gives the temperature conditions. These conditions are equivalent to Eq. (3) after deleting the thermal diffusion and reaction terms. Noting that the steady-state temperature gradient at the flame edge is almost zero, this condition can be expressed in the form

$$iI\omega\rho^{(0)}\hat{T}^{(1)} + \rho^{(0)}u_i^{(0)}\hat{T}_{,i}^{(1)} - iI\omega \frac{\gamma - 1}{\gamma} \hat{p}^{(1)} = G_{10} \quad (39)$$

with

$$G_{10} = -\{\hat{u}\hat{\rho}^{(1)}\hat{T}^{(1)} + \hat{\rho}^{(0)}\hat{u}_i^{(1)}\hat{T}_{,i}^{(1)} + \hat{\rho}^{(1)}u_i^{(0)}T_{,i}^{(1)}\}$$

Since the flux of each reactant species is always a fixed fraction of the total flux, the fuel mass flux fraction m_f can be derived from Eq. (4) as

$$\rho u_i Y_{,i} - Y_{,11} = 0 \quad (40)$$

For a one-dimensional expression, m_f is given as

$$m_f = Y - \frac{1}{m} \frac{dY}{dy} \quad (41)$$

where m is the mass flux equal to ρv , and assumption of the constant burning rate at an instant has been used. At the surface,

$$\hat{m}_f^{(1)} = \hat{Y}^{(1)} - \frac{1}{m^{(0)}} \frac{d\hat{Y}^{(1)}}{dy} + \frac{1}{m^{(0)2}} \hat{m}^{(1)} \frac{dY^{(0)}}{dy} + G_{11} \quad (42)$$

in which

$$G_{11} = \frac{1}{m^{(0)}} \left[\frac{\hat{m}^{(1)}}{m^{(0)}} \frac{d\hat{Y}^{(1)}}{dy} - \frac{dY^{(0)}}{dy} \left(\frac{\hat{m}^{(1)}}{m^{(0)}} \right)^2 \right]$$

Using the relationship $\hat{m}^{(1)} = \rho_s \hat{r}^{(1)}$ yields

$$\hat{Y}^{(1)} = \frac{d\hat{Y}^{(1)}}{dy} - c_1 \frac{dY^{(0)}}{dy} (\hat{T}_s^{(1)} + G_{12}) \quad (43)$$

with

$$G_{12} = \left(\frac{c_1}{2} - \frac{1}{\bar{T}_s} \right) \hat{T}_+^{(1)2}$$

The normal velocity component is derived from the mass balance condition at the interface such that

$$\hat{v}_+^{(1)} = \left(\frac{E_s}{\bar{T}_s} + 1 \right) \hat{T}_+^{(1)} - \bar{T}_s \hat{p}^{(1)} + G_{13} \quad (44)$$

where

$$G_{13} = c_1 \left(\frac{E_s}{2\bar{T}_s} - 1 \right) \hat{T}_+^{(1)2} + (\hat{T}_+^{(1)} - \hat{v}_+^{(1)}) \left(\hat{p}^{(1)} - \frac{1}{\bar{T}_s} \hat{T}_+^{(1)} \right)$$

Moreover, the parallel velocity component may be obtained using the Taylor series expansion about the surface where the no-slip condition must be valid. Thus,

$$\hat{u}_+^{(1)} = \frac{1}{iI\omega\beta} \frac{\partial u^{(0)}}{\partial y} \Big|_+ \hat{r}^{(1)} + G_{13} \quad (45)$$

with

$$G_{14} = \frac{1}{iI\omega\beta} \frac{\partial \hat{u}^{(1)}}{\partial y} \Big|_+ \hat{r}^{(1)} - \frac{1}{2I^2\omega^2\beta^2} \frac{\partial^2 u^{(0)}}{\partial y^2} \Big|_+ \hat{r}^{(1)2}$$

Note that $G_7 \sim G_{14}$ are valid only for $I = 2$. For higher order systems, Eqs. (37)-(39) and Eqs. (43)-(45) are used as boundary conditions to solve Eqs. (28)-(32). It is necessary to have more conditions for the density at both sides for better solutions, and the pressure fluctuation has to be forced at the flame edge. In the case of the second order time-independent system, care must be taken to use boundary equations (35) and (39).

3. NUMERICAL METHOD

Each set of governing equations, subject to appropriate boundary conditions, is solved using the Galerkin finite element method. The boundary equations are imbedded in the total matrix equations by means of Lagrange multiplier λ_γ , such that the overall global matrix has the form

$$\begin{bmatrix} iI\omega A_{\alpha\beta} + B_{\alpha\beta} & q_{\gamma\alpha} \\ q_{\gamma\beta} & 0 \end{bmatrix} \begin{bmatrix} X_\beta \\ \lambda_\gamma \end{bmatrix} = \begin{bmatrix} G_\alpha \\ b_\gamma \end{bmatrix} \quad (46)$$

in which X_β represents the solution vector, $X_\beta = [\rho_\beta, u_{\beta 1}, T_\beta, Y_\beta, P_\beta]$, and G_α denotes the inhomogeneous source terms valid for the second order. The second row, $q_{\gamma\beta} X_\beta = b_\gamma$, represents the boundary equations, where $\gamma = 1, 2, \dots, m$, m being the number of equations. The solution of Eq. (46) at a given frequency is obtained by imposing the Dirichlet condition of the pressure at the flame edge. Note that the first row of Eq. (46) gives the eigenvalue problem when $G_\alpha = 0$ and from which the natural frequency of the system is obtained. The finite element formulation contains two different kinds of test function used to represent the volume and surface integrals in the domain. The total number of field variables would be reduced by one if the density or pressure were eliminated using the perfect gas law. However, the stability of the matrix is doubtful. Before calculations, the following is expected: since the Mach number is generally very small, the coefficient of the pressure term in Eq. (2) dominates the system unless the frequency considered is large enough such that other coefficients containing the

frequency factor become comparable in magnitude. Therefore, in lower frequencies the pressure gradient has to be negligible, thus resulting in constant pressure. On the contrary, the gradient will become significant in higher frequencies; this results in pressure variance. In the latter case, severe pressure changes will occur if unbounded at the solid surface. Note that care must be exercised in expanding Eq. (9) due to the appearance of the exponential growth effect. For the steady-state case, as mentioned earlier, we calculate the eigenvalue B in which necessary initial conditions are satisfied. However, as will be discussed later, the eigenvalue is referred from the result of reference [21] for this study.

4. DISCUSSION

All the perturbed governing equations in the higher order systems having variable coefficients basically depend on the steady-state temperature distribution in the domain, as shown in Eqs. (15)-(18). Figure 1 shows a typical steady-state distribution of the field variables, including the reaction rate for an adiabatic flame with a second order chemical reaction mentioned in T'ien [21]. For verification, the following parameters are utilized: $z = 1$, $\delta = 0$, $T_c = 0.15$, $\bar{T}_s = 0.35$, $\xi = 1$, $E = 10$, $E_s = 4$, $L = 0.15$, and $\beta = 1000$. The other parameters are taken from Flandro [23] and are as follows: $\gamma = 1.2$, $M_b = 0.003$, $u_c = 1.0$, $R_c = 5.0$, $Pr = 1.0$, and $h = 1.3$. Representative dimensional parameters corresponding to the dimensionless values are given in Table 1.

Table 1 Typical value and range of parameters

Parameter	Typical Value	Range	Physical Variable	Typical Value
ρ_s	1000	250-1000	-g/cm ³	1.5
ρ_g	1	-	g/cm ³	1.5×10^{-3}
T_c	0.15	-	^o K	300
T_s	0.35	-	^o K	700
T_f	1.0	-	^o K	2000
E	10	4-15	cal/gmole	40×10^3
E_s	4	2-10	cal/gmole	16×10^3
C_p	-	-	cal/g ^o k	0.33
C_s	-	-	cal/g ^o k	0.33
k_g	-	-	cal/cm ^o ksec	5×10^{-4}
k_s	-	-	cal/cm ^o ksec	5×10^{-4}
m_0	1	-	g/cm ² sec	0.4
P_0	1	-	atm	9.5
r	2	0.5-2	-	-
Y_f	0.5	0.4~0.85	-	-
ω	-	10^{-3} - 10^2	H ₂	-
γ	1.4	-	-	-
ΔH	0.15	0.05-0.3	cal/gmole	2.8×10^3

As mentioned earlier, the natural frequency of the given system is obtained from the homogeneous solution of the total matrix equation (46) without the boundary conditions. As previously suggested [28], the result shows that the active energy transfer between the acoustic wave and the combustion process occurs mostly in a lower frequency range which leads to acoustic instability. In this study, most of the frequencies are clustered in $\omega < 20$; hence, the frequency range of interest is chosen between $\omega = 10^{-3}$ and $\omega = 10^2$ and it extends up to $\omega = 500$.

The thickness of the burning zone is assumed to be negligibly small compared with the wavelength of the acoustic oscillation; thus, the pressure is approximately uniform throughout the domain of study and varies only with time. From this point of view, one of the most significant aspects of the present study is the fact that the oscillating pressure is no longer taken to be uniform at any instant, but is regarded as a spatially nonhomogeneous time-dependent source term. Consequently, it allows us to investigate the response of a specific propellant at significantly high frequencies and to find the response in the long flame of a double-base propellant. The frequency limit has usually been determined by the reciprocal of the characteristic time in Eq. (16). However, it is inversely proportional to the square of the burning rate; therefore, the limit cannot be constant, but varies with the pressure fluctuations. This argument is verified in the present study using two different cases: (1) increasing the order of perturbation decreases the upper limit of the frequency and (2)

increasing the flame thickness also decreases the upper limit. Flandro [23] defines the non-uniform pressure coefficient explicitly in terms of the position and incident angle outside the combustion region; however, further discussion concerning this subject is not available.

First, we attempt to verify the results of the new model in the one-dimensional problem. The calculation is actually conducted in multiple dimensions, but the boundary conditions are chosen approximately as if the gas flow seems to act one-dimensionally. Data at the center nodes of the domain are used to evaluate the results. Figure 2 demonstrates distributions of component fluctuations in the first order at $\omega = 1$. The results are comparable to those of T'ien [21]. In Fig. 2, it is also shown that the highest temperature fluctuations arise at the point where the maximum reaction occurs. Other field variables have their maximum/minimum values at the point where the gradient of the reaction is maximized. The temperature amplification at the surface changes the burning rate in Eq. (36), while the velocity at the flame edge represents the acoustic admittance, whose magnitude and sign indicate the instability of the system. Note that the pressure remains constant, implying that the acoustic wavelength is larger than the flame thickness in this case; consequently, the imaginary part of the velocity approaches a constant slope at the edge.

Distributions of the field variables against frequency for the first order are calculated and shown in Figs. 3-7. The amplitude of the pressure disturbance playing the role of the

forcing function is set to unity at the flame edge. The results show that, at certain lower frequencies ($\omega < 10$), the pressure is constant but varies in the higher region ($\omega > 10$). Thus, the limit of the constant pressure assumption is clearly recovered. General trends show that the distribution profiles are divided roughly into two groups at about $\omega = 1$; one is for $\omega < 1$ and the other for $\omega > 1$. In the lower frequencies (quasi-steady region), the variables, keeping similar distribution profiles, change their magnitude negligibly along the frequency. This trend is also true for the higher frequencies up to $\omega = 100$. The only exception is at $\omega = 1$, and it gives very different distribution profiles among others. The figures also reveal that the results are closely related to the chemical reaction distribution.

The overall density distributions based on a second order chemical reaction are depicted in Fig. 3. The changes in magnitude along the flame are more significant in higher frequencies than in lower frequencies. These changes seem to be directly related to the fuel species (Fig. 7) and implicitly related to the temperature (Fig. 6). The imaginary parts of the density represent the phase shift from the incident wave, and these are almost zero except for $\omega = 1$.

At the surface, positive magnitude implies a stagnant phenomena caused by decreasing the velocity, although the mass flux increases at a higher pressure level. Special attention is invited to the profile at $\omega = 1$, where the profile is entirely different from others and some portions of the flame have negative amplitudes. The mass balance predicts a faster velocity

at the negative portion, as shown in Fig. 4. It can be said that the combustion system is most sensitive to the pressure fluctuation at $\omega = 1$ in the frequency region considered. If the upper limit of the frequency is extended, the profile is reversed, but with a similar trend of periodicity. A simple chemical reaction model restricts a realistic discussion in detail since, for most propellants, it is more complex than it implies.

The normal velocity distributions are shown in Fig. 4. Two kinds of profile are obvious: one with positive slope and one with negative slope. The latter contains most of the distributions in the lower frequency region, with some exceptions. Note that a different profile appears at $\omega = 1$. Rearranging the real part of the velocity at the flame edge gives the distribution of the acoustic admittance, whose magnitude and sign indicate the amplifications or damping ability of the flame subject to the acoustic disturbance (Fig. 5). Figure 5 reveals a resonance in the condensed phase near $\omega = 0.01$, indicating that the system is unstable. This verifies the early result of Denison and Baum [4]. Some negative peaks exist at the other frequencies, indicating that the resonance in the gas phase tends to damp the oscillatory motion. Figure 5 also shows the system to be unstable at most higher frequency regions. The real part of the burning rate in Eq. (36) gives a similar trend to the acoustic admittance at the quasi-steady region, although the magnitude is significantly different. But these trends differ from each other at the higher region, as indicated in [21].

Thus, the burning rate is not representative as a stability measure for a higher oscillatory case. Over $\omega = 100$, the profile tends to have a second mode oscillation as the pressure varies in the flame zone.

Figures 6 and 7 illustrate the temperature and fuel species. At the lower frequency region, changes of magnitude are insignificant while at the higher region, such changes become significant. Because the temperature increases with fuel consumption, the distribution curves are in opposing directions. It is also seen that linearly diminishing the fuel affects the temperature changes slowly. Note that the difference in the fuel amount at the surface implies the change in the burning rate affected by the disturbances. Significant changes of variables are also given at $\omega = 1$.

In the first order system, the constant pressure field is valid until $\omega = 10$; above that frequency the pressure varies. This result gives the limit of the uniform pressure assumption. Furthermore, it shows that up to $\omega = 100$, the magnitude grows linearly starting from the flame edge where the Dirichlet condition is imposed, and then begins to oscillate.

As previously indicated, each variable of the second order response to acoustic disturbance has two components: one time-dependent component that oscillates at twice the fundamental frequency and one that is time-independent. The latter represents a shift in the mean value, thus causing a shift of the mean burning rate. The right-hand side of the second order total matrix equation consists of corresponding nonlinearities in terms

of the product of two first order variables. These nonlinearities function as source terms. The computations are performed for the time-independent component using the Dirichlet condition of the pressure to be unity at the flame edge. Distributions of the field variables as well as the shift of the burning rate are investigated. Figure 8 shows typical distribution profiles in the second order at $\omega = 1$; at this frequency, the constant pressure is retained.

The variables follow trends similar to those of the first order, although the amplifications affected by the existence of nonlinearities in the higher order are different. The trends still show a small discrepancy at the flame edge as in the first order. Figures 9-12 illustrate the behavior of each variable against the frequency. The general tendency of the second order is to affect the flame toward stability in the lower frequency region. Note that the upper limit of the frequency for constant pressure assumption has to be reduced by one half. The computational results show that the pressure changes from $\omega = 5$, which is half of the limit frequency in the first order. Thus, the limit should be determined by considering the order of perturbation involved in the calculations.

At $\omega < 100$, the variables have the same order of magnitude as that of the pressure imposed. However, the velocity changes significantly from $\omega = 1$ due to the pressure change from that frequency. Thus, a higher order effect may not be negligible unless the perturbation parameter ϵ has an order of magnitude less than the reciprocal of the highest order in the problem. At

lower frequencies, as shown in the first order, the distribution profiles are very similar; at higher frequencies, they differ from each other.

Finally, the burning rate offset is calculated and given in Fig. 13. The offset is relatively small in the quasi-steady region, but increases with oscillatory motion along the frequencies. It has a negative sign in the entire frequency range, indicating a decrease of the burning rate subject to the acoustic pressure oscillations. This verifies the experimental result of Price [39], and the averaged curve looks similar to the analytical results of Friedly and Petersen [10].

Parameter studies are conducted for the first order and summarized as follows. Decreasing the density ratio β affects the variables shifted slightly to the negative direction, keeping the distribution profiles constant. Changing the latent heat of solid L exerts a negligible effect on the variables, but a very small value of L shifts the system toward instability. Increasing the surface activation energy E_s or the gas phase activation energy E reduces the magnitude of the variables, keeping the same profiles. Changes of the rate constant and viscosity effect coefficient strongly affect the system, such that every aspect discussed herein will change.

The present study could be extended to the multi-dimensional case by introducing the appropriate axial mean flow field [46]. It is well recognized that fluctuation of the gas velocity parallel to the propellant surface affects the burning rate in terms of velocity coupling; therefore, this quantity must be

considered together with pressure coupling for a satisfactory measure of stability. A simple calculation has been accomplished using the artificial axial flow velocity in Eq. (22). However, difficulties of the boundary conditions could not be eliminated. A test run shows that the existence of a small amount of the axial flow reduces the range of dispersion of the variable distribution profile from each other in the frequency region that leads the system toward stability.

5. CONCLUSION

A multi-dimensional numerical model for the premixed flame acoustic instability is proposed and solved using the finite element method. The governing equations are perturbed to the second order and formulated with Galerkin finite elements. The gaseous flame is assumed to be simple and homogeneous, and the Arrhenius manner of decomposition is implemented with no condensed phase reaction. The results have direct bearing on the validity of published theories of solid propellant combustion instability at the lower frequency region where the uniform pressure is valid. Extended studies are made on the higher frequency region and the results are discussed. Under the restricted boundary conditions, the following conclusions, based on numerical calculations, are reached:

- (1) The pressure is assumed to vary in the domain of study, and calculations based on nonuniform pressure indicate that for $\omega > 10$, there is a significant deviation from the uniform pressure assumption for the first order.

- (2) For the second order system, such deviation occurs at a lower frequency which is half of the first order frequency limit.
- (3) Investigation of the distribution of variables shows that the acoustic instability is likely to be most critical at $\omega = 1$, while the acoustic admittance at the flame edge indicates a negative sign.
- (4) The oscillatory amplification or damping ability of the flame is recovered in the quasi-steady region and, at a higher frequency, moderate amplification effects are obtained.
- (5) The burning rate is directly related to the acoustic admittance only at the lower frequency region and its negative offset phenomena have been valid in the second order perturbation study.
- (6) Second order effects may cause the instability to be more critical in some cases and negligible in others.
- (7) Multi-dimensional instability calculations can be achieved using this model so far as a realistic mean flow field is clarified with proper boundary conditions.

REFERENCES

1. Cheng, Sin-I, "High Frequency Combustion Instability in Solid Propellant Rockets", Jet Propulsion, 1954, Part I, pp. 27-32, Part II, pp. 102-109.
2. Hart, R. W. and McClure, F. T., "Combustion Instability: Acoustic Interaction with a Burning Propellant Surface", J. Chem. Phys., Vol. 30, Sept. 1959, pp. 1501-1514.
3. McClure, F. T., Hart, R. W., and Bird, J. F., "Acoustic Resonance in Solid Propellant Rockets", J. Appl. Phys., Vol. 31, Apr. 1960, pp. 884-896.
4. Denison, M. R. and Baum, E., "A Simplified Model of Unstable Burning in Solid Propellants", ARS J., Vol. 31, Aug. 1961, pp. 1112-1122.
5. Cheng, Sin-I, "Unstable Combustion in Solid Propellant Rocket Motors", 8th Symposium (Int.) on Combustion, Williams and Wilkins, 1962, pp. 81-96.
6. Williams, F. A., "Response of a Burning Solid to Small Amplitude Pressure Oscillations", J. Appl. Phys., Vol. 33, Nov. 1962, pp. 3153-3166
7. Cantrell, R. H., Hart, R. W., and McClure, F. T., "Linear Acoustic Gains and Losses in Solid Propellant Rocket Motors", AIAA J., Vol. 2, No. 6, June 1964, pp. 1100-1105.
8. Hart, R. W. and McClure, F. T., "Theory of Acoustic Instability in Solid Propellant Rocket Combustion", 10th Symposium (Int.) on Combustion, 1965.
9. Friedly, J. C. and Petersen, E. E., "Influence of Combustion Parameters on Instability in Solid Propellant Motors, Part I: Development of Model and Linear Analysis", AIAA J., Vol. 4, No. 9, Sept. 1966, pp. 1605-1610.
10. Friedly, J. C. and Petersen, E. E., "Influence of Combustion Parameters on Instability in Solid Propellant Motors, Part II: Nonlinear Analysis", AIAA J., Vol. 4, No. 11, Nov. 1966, pp. 1932-1937.
11. Culick, F. E. C., "Acoustic Oscillations in Solid Propellant Rocket Chambers", Astronautica Acta, Vol. 12, Feb. 1966, pp. 114-126.
12. Culick, F. E. C., "Calculations of the Admittance Function for a Burning Surface", Astronautica Acta, Vol. 13, No. 3, 1967, pp. 221-237.

13. Culick, F. E. C., "A Review of Calculations for Unstable Burning of a Solid Propellant", AIAA J., Vol. 6, Dec. 1968, pp. 2241-2254.
14. Culick, F. E. C., "Nonlinear Behavior of Acoustic Waves in Combustion Chambers", CPIA Pub. 243, 10th JANNAF Combustion Meeting, Vol. 1, CPIA Pub. 243, 1973, pp. 417-436.
15. Ibiricu, M. M. and Krier, H., "Acoustic Amplification During Solid Propellant Combustion", Combustion and Flame, Vol. 19, 1972, pp. 379-391.
16. Williams, F. A., "Quasi-Steady Gas-Phase Flame Theory in Unsteady Burning of a Homogeneous Solid Propellant", AIAA J., Vol. 11, 1973, pp. 1328-1330.
17. Levine, J. N. and Culick, F. E. C., "Nonlinear Analysis of Solid Rocket Combustion Instability", AFRPL TR-74-45, Oct. 1974.
18. Micci, M. M., Caveny, L. H., and Summerfield, M., "Solid Propellant Rocket Motor Response Evaluated by Means of Force Longitudinal Waves", AIAA paper 77-974, July 1977.
19. King, M. K., "Modeling of Pressure-Coupled Response Functions of Solid Propellants", 19th Symposium (Int.) on Combustion, The Combustion Institute, 1982, pp. 707-715.
20. Krier, H., T'ien, J. S., Sirignano, W. A., and Summerfield, M., "Nonsteady Burning Phenomena of Solid Propellant Theory and Experiments", AIAA J., Vol. 6, No. 2, 1968, pp. 278-285.
21. T'ien, J. S., "Oscillatory Burning of Solid Propellants Including Gas Phase Time Lag", Combustion Science and Technology, Vol. 5, 1972, pp. 47-54.
22. Flandro, G. A., "Solid Propellant Acoustic Admittance Correlations", Vibration and Sound, Vol. 36, 1974, pp. 297-312.
23. Flandro, G. A., "Nonlinear Time-Dependent Combustion of a Solid Rocket Propellant", 19th JANNAF Combustion Meeting, Oct. 1982.
24. Micheli, P. L. and Flandro, G. A., "Nonlinear Stability for Tactical Motors Vol. III - Analysis of Nonlinear Solid Propellant Combustion Instability", AFRPL TR-85-017, Feb. 1986.
25. Chung, T. J., Hackett, R. M., Kim, J. Y., and Radke, R., "A New Approach to Combustion Instability Analysis for Solid Propellant Rocket Motors", 19th JANNAF Combustion Meeting, Oct. 1982.

26. Chung, T. J. and Kim, P. K., "A Finite Element Approach to Response Function Calculations for Solid Propellant Rocket Motors", AIAA paper 84-1433, June 1984.
27. Chung, T. J. and Kim, J. Y., "Two-Dimensional Combined Model Heat Transfer by Conduction, Convection, and Radiation in Emitting, Absorbing, and Scattering Media - Solution by Finite Elements", J. Heat Transfer, Vol. 106, 1984, pp. 448-452.
28. Chung, T. J. and Kim, P. K., "Unsteady Response of Burning Surface in Solid Propellant Combustion", AIAA paper 85-0234, Jan. 1985.
29. Chung, T. J., Finite Element Analysis in Fluid Dynamics, McGraw-Hill Book Co., 1978.
30. Williams, F. A. and Lengelle, G., "Simplified Model for Effect of Solid Heterogeneity on Oscillatory Combustion", Astronautica Acta, Vol. 14, Jan. 1968, pp. 97-118.
31. Condon, J. A., Osborn, J. R., and Glick, R. L., "Statistical Analysis of Polydisperse, Heterogeneous Propellant Combustion: Nonsteady-State", 13th JANNAF Combustion Meeting, CPIA Pub. 281, Vol. 2, 1976, pp. 209-223.
32. Beckstead, M. W., "Combustion Calculations for Composite Solid Propellants", 13th JANNAF Combustion Meeting, CPIA Pub. 281, Vol. 2, 1976, pp. 299-312.
33. Cohen, N. S., "Response Function Theories that Account for Size Distribution Effects - A Review", AIAA J., Vol. 19, No. 7, July 1981, pp. 907-912.
34. Culick, F. E. C., "Stability of Longitudinal Oscillations with Pressure and Velocity Coupling in a Solid Propellant Rocket", Combustion Science and Technology, Vol. 2, 1970, pp. 179-201.
35. Micheli, P. L., "Investigation of Velocity Coupled Combustion Instability", Aerojet Solid Propellant Co., AFRPL TR-76-100, Jan. 1977.
36. Condon, J. A., "A Model for the Velocity Coupling Response of Composite Propellant", 16th JANNAF Combustion Meeting, CPIA Pub. 308, Dec. 1979.
37. Beckstead, M. W., "Report of the Workshop on Velocity Coupling", 17th JANNAF Combustion Meeting, CPIA pub. 324, Nov. 1980, pp. 195-210.

38. Brown, R. W., Waugh, R. C., Willoughby, P. G., and Dunlop, R., "Coupling between Velocity Oscillations and Solid Propellant Combustion", 19th JANNAF Combustion Meeting, CPIA Pub. 366, Vol. 1, Oct. 1982, pp. 191-208.
39. Price, E. Q., Mathes, H. B., Crump, J. E., and McGie, M. R., "Experimental Research in Combustion Instability of Solid Propellants", Combustion and Flame, Vol. 5, 1961, pp. 149-162.
40. Coates, R. L., Horton, M. D., and Ryan, N. W., "T-Burner Method of Determining the Acoustic Admittance of Burning Propellants", AIAA J., Vol. 2, No. 6, June 1964, pp. 1119-1122.
41. Coates, R. L., Cohen, N. S., and Harvill, L. R., "An Interpretation of L^* Combustion Instability in Terms of Acoustic Instability Theory", AIAA J., Vol. 5, No. 5, May 1967, pp. 1097-1102.
42. Brown, R. S., Culick, F. E. C., and Zinn, B. T., "Experimental Method for Combustion Admittance Measurements", Experimental Diagnostics in Combustion of Solids: AIAA Progress in Astronautics and Aeronautics, Vol. 63, edited by T. L. Boggs and B. T. Zinn, AIAA, NY, 1979, pp. 191-220.
43. Baum, J. D., Levine, J. N., and Lovine, R. L., "Pulse-Triggered Instability in Solid Rocket Motors", AIAA J., Vol. 22, No. 10, Oct. 1984, pp. 1413-1419.
44. Lovine, R. L., Baum, J. D., and Levine, J. N., "Ejecta Pulsing of Subscale Solid Propellant Rocket Motors", AIAA J., Vol. 23, No. 3, Mar. 1985, pp. 416-423.
45. Caveny, L. H., Collins, K. L., and Cheng, S. W., "Direct Measurements of Acoustic Admittance Using Laser Doppler Velocimetry", AIAA J., Vol. 19, No. 7, July 1981, pp. 913-917.
46. Chung, T. J. and Sohn, J. L., "Interactions of Coupled Acoustic and Vortical Instability", AIAA J., Vol. 24, No. 10, Oct. 1986, pp. 1582-1596.

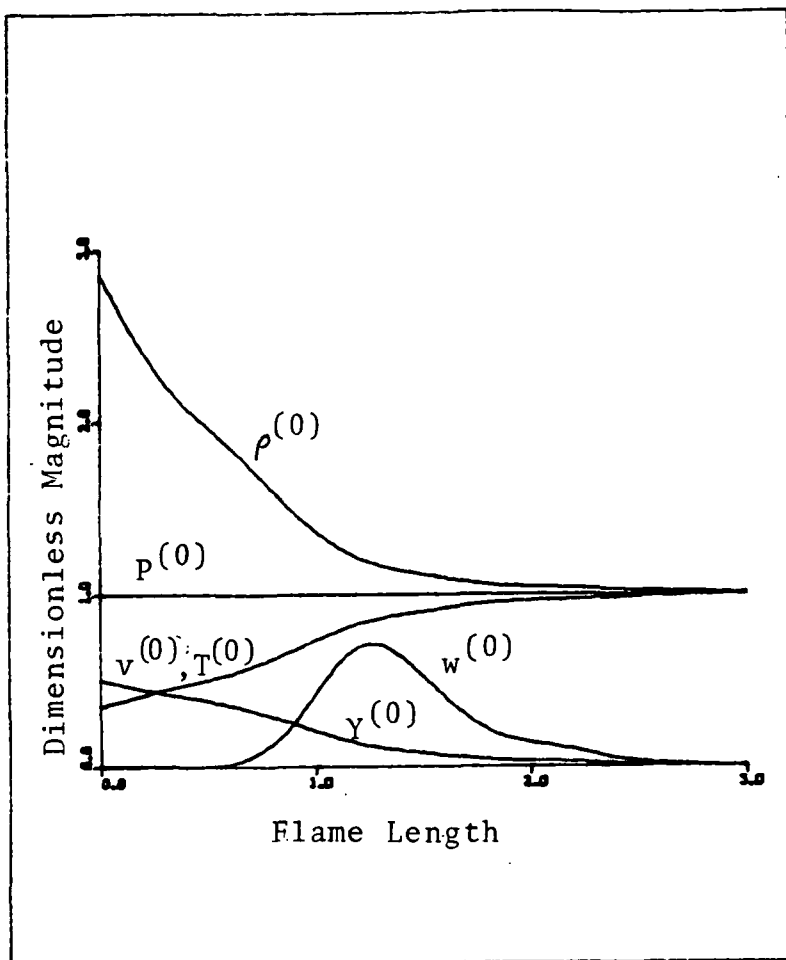


Fig. 1 Steady-state distributions of field variables in flame zone. Parameters used in calculations are given in Table 1, with $Pr = 1$ and $M_b = 0.003$. Mean values at the flame edge are used to non-dimensionalize the variables. The higher order calculations are based on this result.

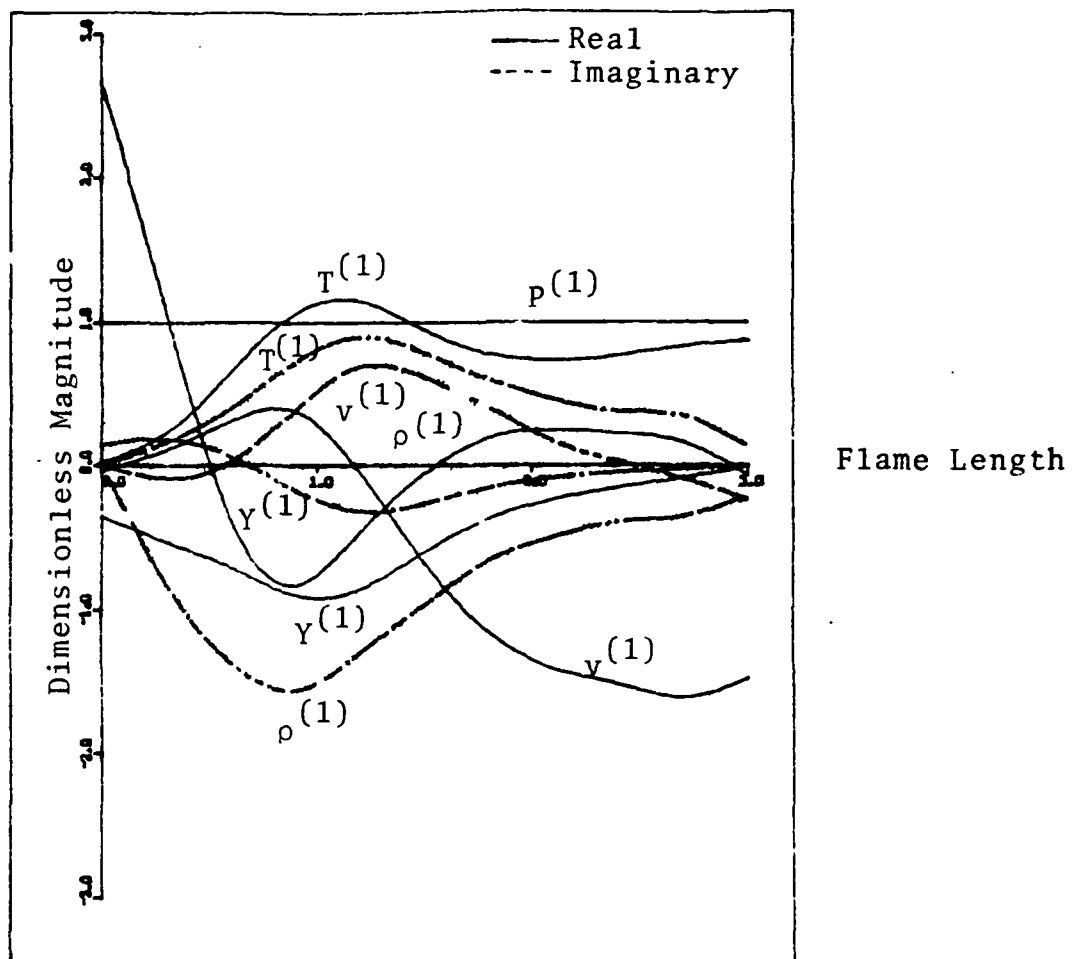


Fig. 2 First order distributions of field variables at $\omega = 1$.

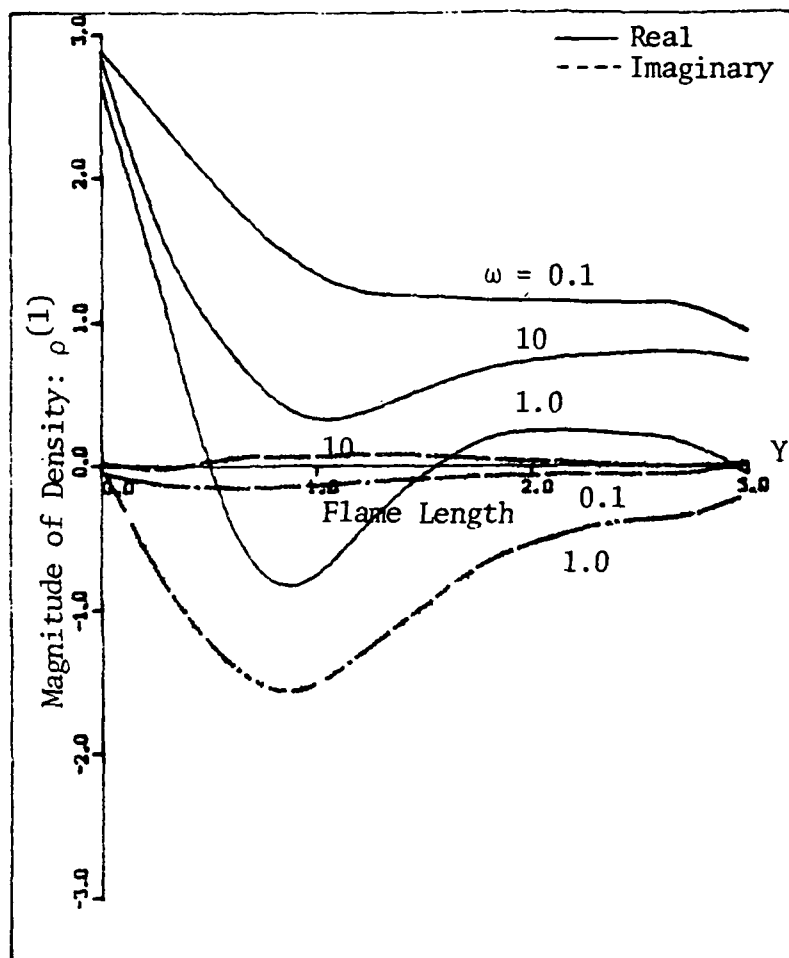


Fig. 3 First order density distributions vs. frequency.

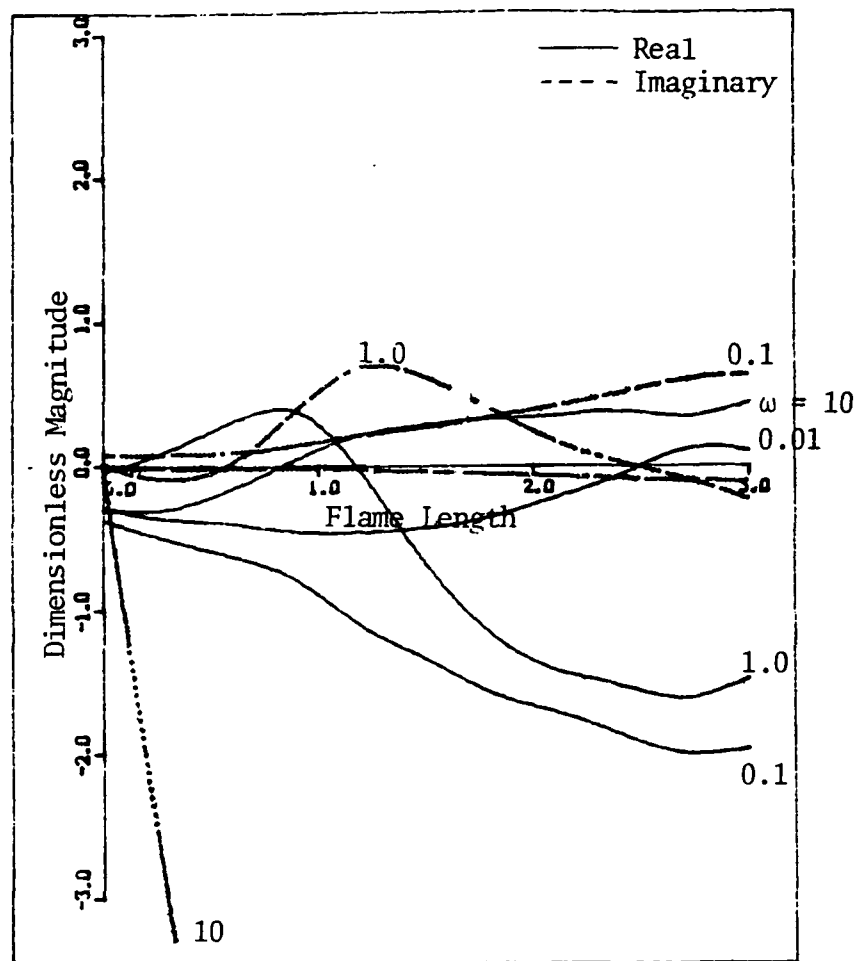


Fig. 4 First order velocity distributions vs. frequency.

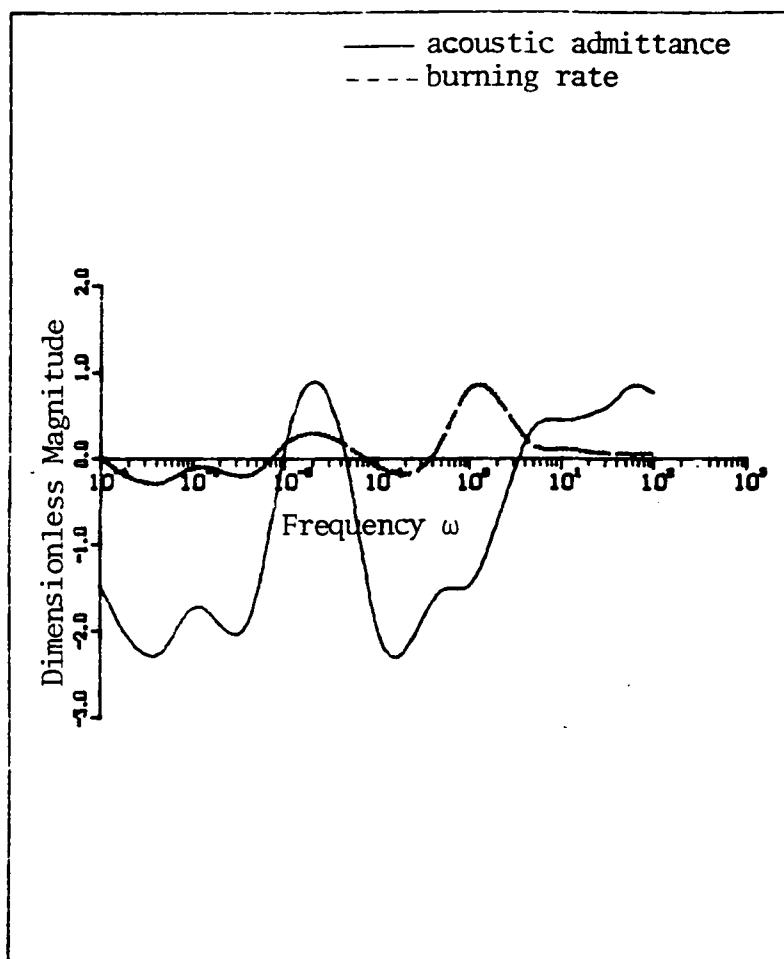


Fig. 5 Acoustic admittance and burning rate vs. frequency.

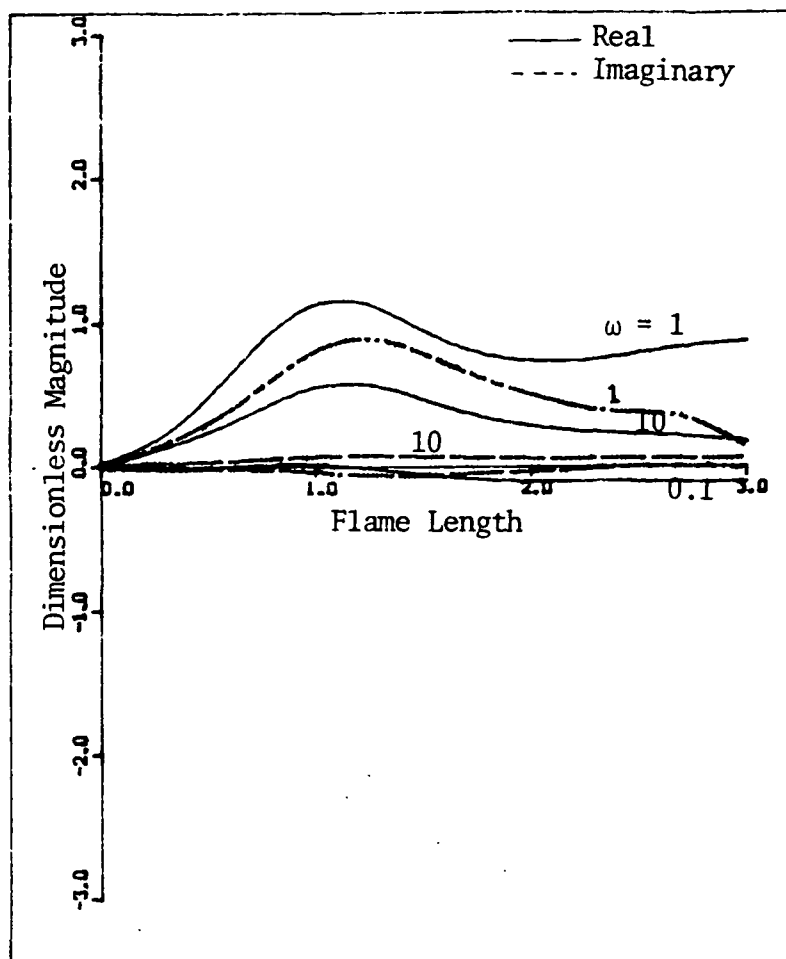


Fig. 6 First order temperature distributions vs. frequency.

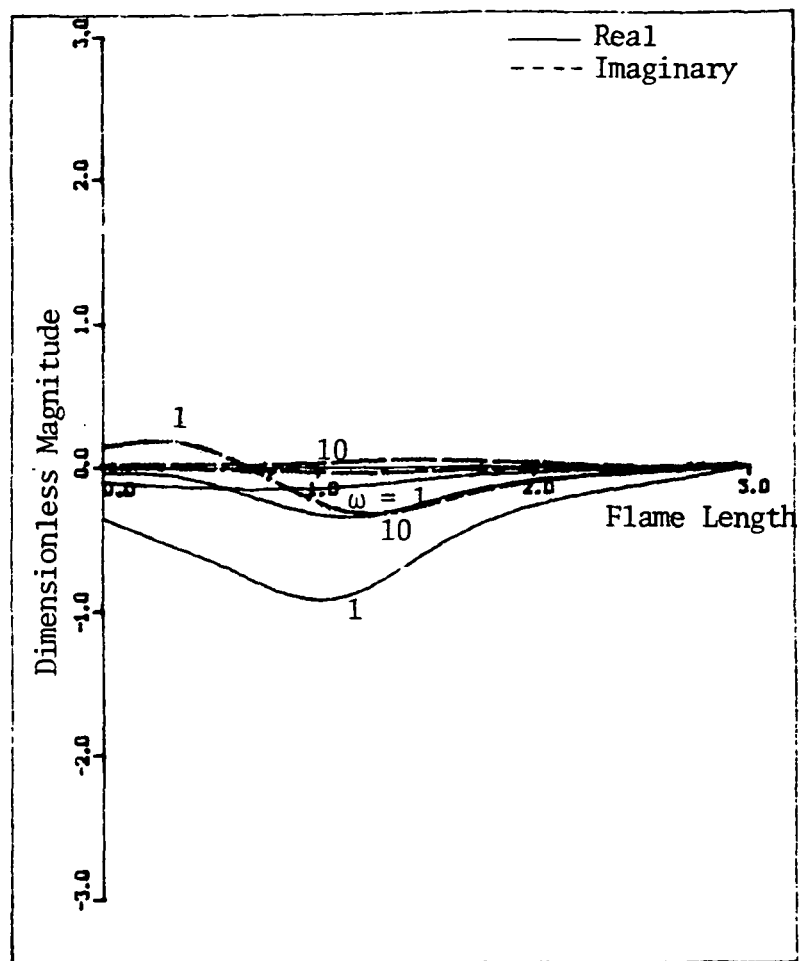


Fig. 7 First order species (fuel) distributions vs. frequency.

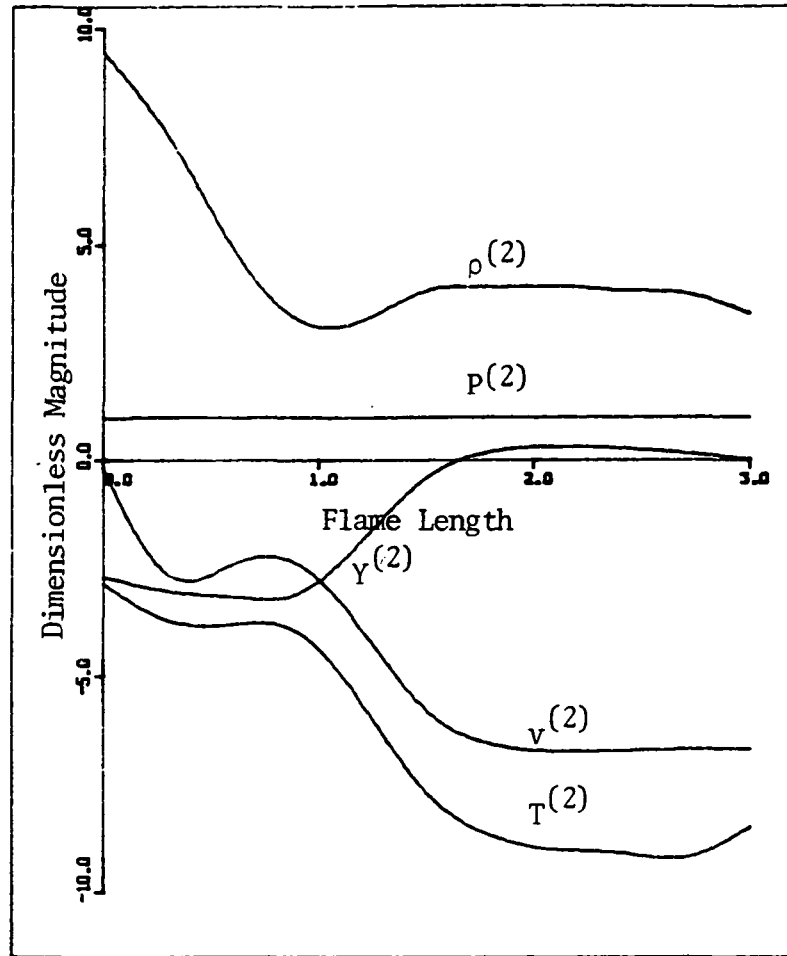


Fig. 8 Second order time-independent distributions of field variables at $\omega = 1$.

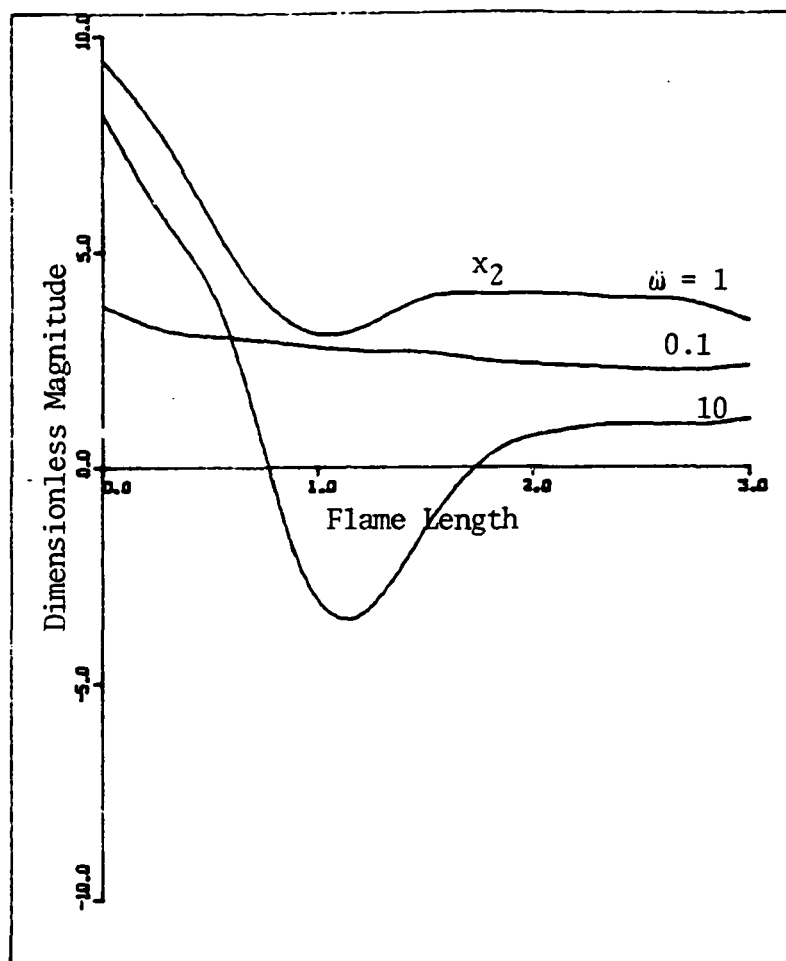


Fig. 9 Second order time-independent density distributions vs. frequency.

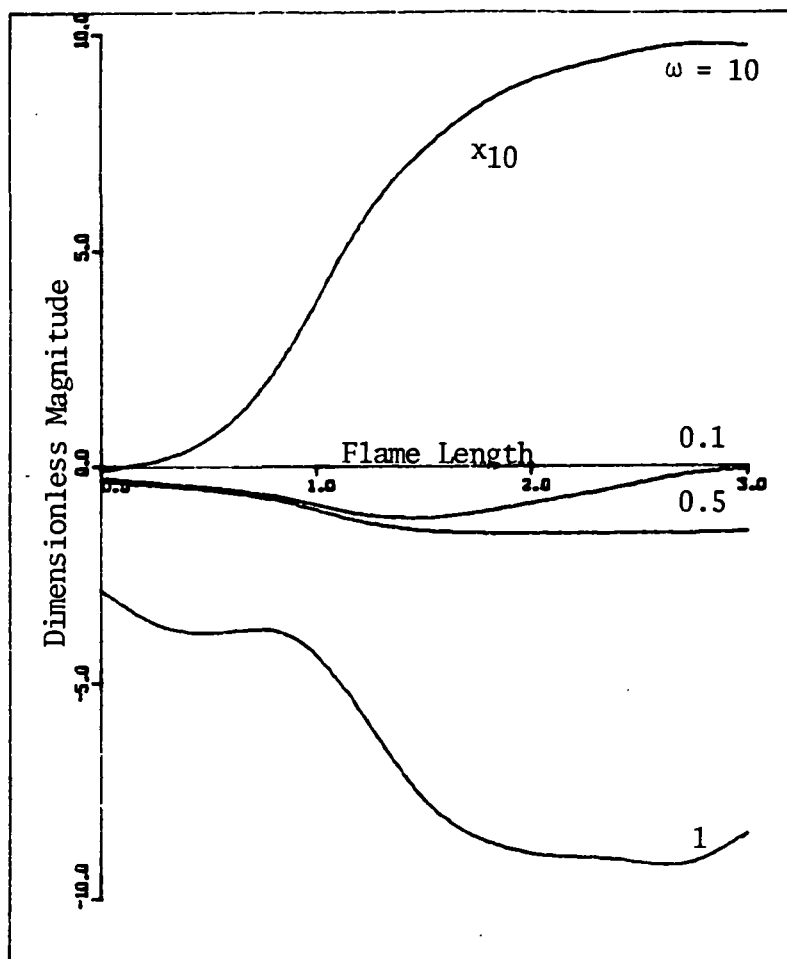


Fig. 10 Second order time-independent velocity distributions vs. frequency.

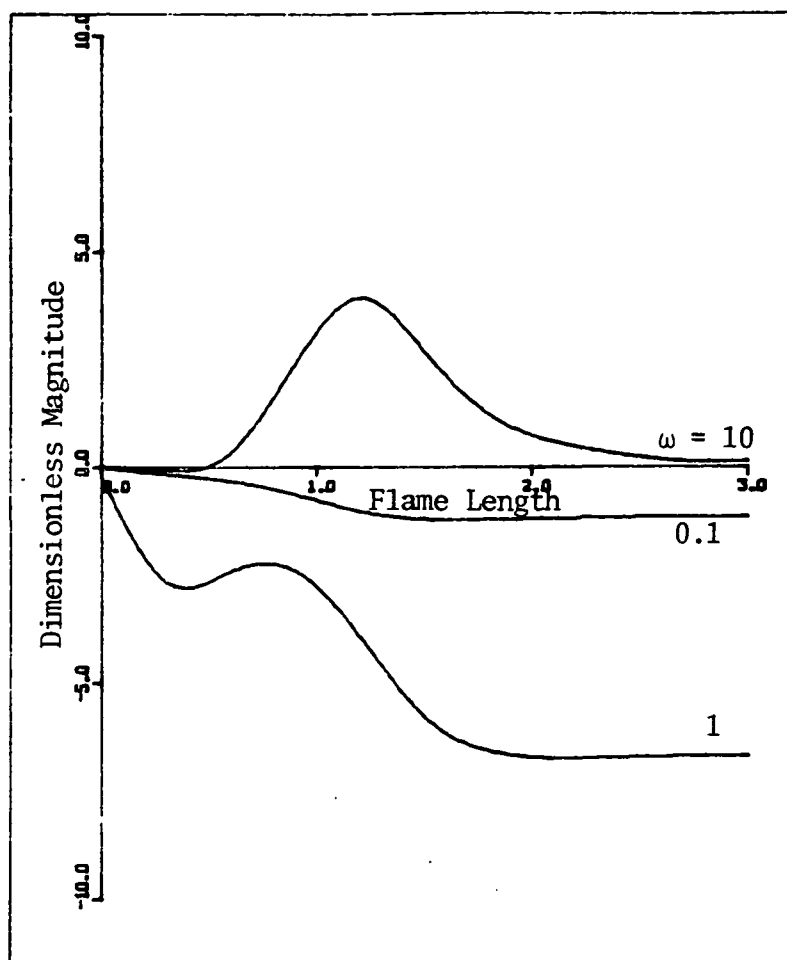


Fig. 11 Second order time-independent temperature distributions vs. frequency.

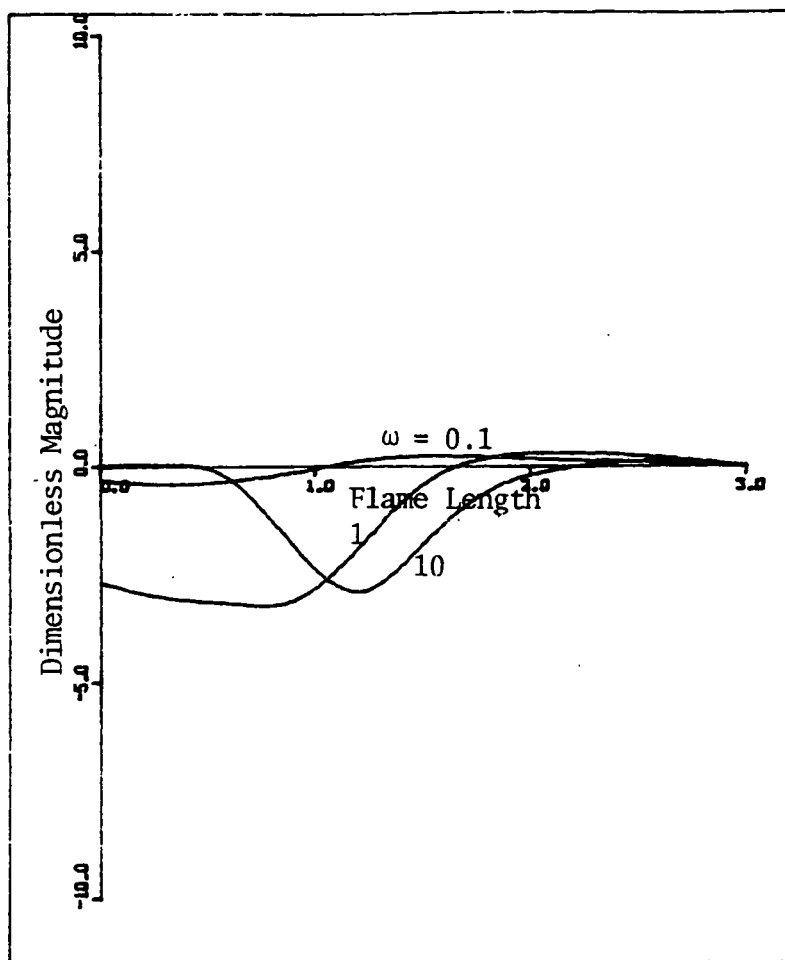


Fig. 12 Second order time-independent species (fuel) distributions vs. frequency.

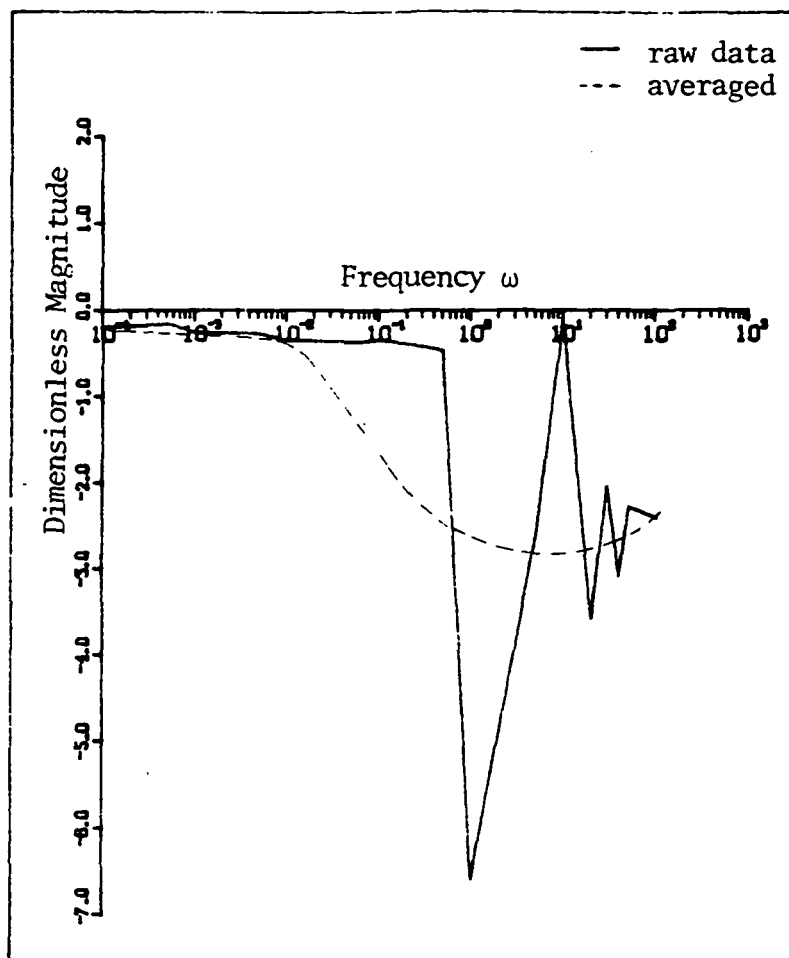


Fig. 13 Offset in burning rate for the second order time-independent system. Calculations are from Eq. (36) using Figs. 6 and 11. The negative sign in all the frequency region indicates that the burning rate always decreases by the acoustic pressure oscillations reported by Price [39]. The average trend is comparable to the analytical result of Friedly and Petersen [10].